

Universal properties of Wigner delay times and resonance widths of tight-binding random graphs

K. B. Hidalgo-Castro,¹ L. A. Razo-López,² A. M. Martínez-Argüello,^{1,*} and J. A. Méndez-Bermúdez^{1,3}

¹*Instituto de Física, Benemérita Universidad Autónoma de Puebla, Puebla 72570, Mexico*

²*Université Côte d'Azur, CNRS, Institut de Physique de Nice (INPHYNI), Nice, France*

³*Escuela de Física, Facultad de Ciencias, Universidad Nacional Autónoma de Honduras, Honduras*

The delay experienced by a probe due to interactions with a scattering media is highly related to the internal dynamics inside that media. This property is well captured by the Wigner delay time and the resonance widths. By the use of the equivalence between the adjacency matrix of a random graph and the tight-binding Hamiltonian of the corresponding electronic media, the scattering matrix approach to electronic transport is used to compute Wigner delay times and resonance widths of Erdős-Rényi graphs and random geometric graphs, including bipartite random geometric graphs. In particular, the situation when a single-channel lead attached to the graphs is considered. Our results show a smooth crossover towards universality as the graphs become complete. We also introduce a parameter ξ , depending on the graph average degree $\langle k \rangle$ and graph size N , that scales the distributions of both Wigner delay times and resonance widths; highlighting the universal character of both distributions. Specifically, $\xi = \langle k \rangle N^{-\alpha}$ where α is graph-model dependent.

PACS numbers: 46.65.+g, 89.75.Hc, 05.60.Gg

I. INTRODUCTION

Random graphs have attracted a lot of attention in the last decades, as they have proved to be valuable models for describing complex systems with applications found in a broad variety of areas of research [1–15]. Up to date, many aspects that characterize the behavior of random graphs have been addressed. Those include connectivity and structural properties [1–9], percolation behavior [16], and spectral and eigenfunction statistical properties [17–22]. Based on an electrical analogy, when friction is present in the graphs, further insight into the behavior of random graphs has also been gained by studying the transport properties such as the electrical conductance established between a source node and a sink node assigned to positive and zero potentials respectively [23, 24]. Those properties strongly depend on the graph degree distribution.

Another possibility to characterize the behavior of random graphs has been opened due to the equivalence established between the adjacency matrix and the tight-binding Hamiltonian matrix describing respectively a random graph and an electronic random media, where both matrices are usually represented by sparse random matrices [25–27]. Consequently, this equivalence has also motivated the use of random-matrix theory (RMT) methods and techniques to study spectral, scattering and transport properties of random graphs which in turn provide further information about the structure of the graphs [25–31]. In the latter, the opening of the systems is usually performed by attaching the graphs to the outside by means of perfectly conducting leads, so the fundamental quantity characterizing the scattering processes

within the random media is the scattering matrix; or the S -matrix [32]. It is in this context, for instance, that an isolated-to-metallic crossover as well as universal behavior, well described by RMT, have been observed in the transport properties of Erdős-Rényi random graphs [25] and random geometric graphs [26].

Following the aforementioned equivalence, it is the purpose of the present work to deepen in the understanding of scattering processes in random graphs by studying a transport property of special interest, namely, the delay experienced by an electronic wave due to interactions with a scattering media [33, 34]. That delay is highly related to the internal dynamics inside the media and it is well captured by the so-called Wigner delay time and the resonance widths which represent, respectively, the typical time an electronic wave remains in the scattering media and the lifetime an electronic wave remains in the corresponding resonant state due to the opening of the system. Furthermore, although these quantities have been of great interest in the realm of complex scattering [35–41], they also hold significant importance from an experimental viewpoint as they offer alternative means to characterize systems using scattering measurements, thereby circumventing the need for direct access to wave functions [42–44].

The graph models to be considered below correspond to Erdős-Rényi random graphs and random geometric graphs, including bipartite random geometric graphs. Opposite to Erdős-Rényi graphs, in which nodes are not embedded in a given space, in random geometric graphs nodes are distributed in a geometric space (Euclidian in most cases). Also, random geometric graphs have been introduced as models more suited to describe those real world situations in which a given system is constrained by geometrical spatial bounds such as urban planing [45], species-habitat networks, 5G wireless networks [46], and many others; see e.g. [47] and references therein. More-

* blitzkriegheinkel@gmail.com

over, since a microwave realization of a 2D tight-binding scattering setup is available, our results for random geometric graphs could be straightforwardly verified experimentally in artificial photonic systems [48–52].

The paper is organized as follows. In the next section, the graph models as well as the scattering setup (when the graphs support one-open channel) are introduced. The perfect coupling regime between the graphs and the lead, the scattering phases, the Wigner delay time, and the resonance widths are defined in Sect. III. The numerical results are presented in Sect. IV. Finally, the conclusions are given in Sect. V.

II. GRAPH MODELS AND SCATTERING SETUP

In this work, the focus is paid on the properties of scattering phases, Wigner delay times, and resonance widths of two graph models, namely, Erdős-Rényi graphs (ERGs) and Random Geometric Graphs (RGGs), including a variation of RGGs: Bipartite Random Geometric Graphs (BRGGs). On the one hand, ERGs are composed of N independent vertices, or nodes, connected to each other with probability p , where $p \in [0, 1]$. That is, when $p = 0$ the ERGs consist of N isolated nodes, while when $p = 1$, the graphs are fully connected. On the other hand, RGGs consist of N vertices uniformly and independently distributed in the unit square. Two vertices are connected by an edge if their Euclidean distance is less than or equal to the connection radius $r \in [0, \sqrt{2}]$ [9, 53]. Then, RGGs depend on the parameter pair (N, r) . Meanwhile, BRGGs are composed by N vertices grouped into two disjoint sets, namely, set A with s vertices and set B with $N - s$ vertices, $s \in [1, N - 1]$, where there are no adjacent vertices within the same set. The vertices belonging to both sets are uniformly and independently distributed in the unit square, and two vertices are connected by an edge if their Euclidean distance is less or equal than the connection radius $r \in [0, \sqrt{2}]$ [46]. That is, BRGGs depend on the parameters (N, s, r) . Notice that, given BRGGs of total size N , the parameter s defines the sizes of both sets A and B; hereafter, those graphs will be referred to as BRGGs(s).

The randomly weighted versions of ERGs, RGGs, and BRGGs can be described by the following sparse tight-binding Hamiltonian

$$H = \sum_{n=1}^N h_{nn}|n\rangle\langle n| + \sum_{n,m} h_{nm}(|n\rangle\langle m| + |m\rangle\langle n|), \quad (1)$$

where N is the number of vertices in the graphs, h_{nn} are on-site potentials, and h_{nm} are hopping integrals between sites n and m . In Eq. (1), the second summation runs over all pairs of connected nodes. Furthermore, in Eq. (1) the weights h_{nm} are chosen to be statistically independent random variables drawn from a normal distribution with zero mean $\langle h_{nn} \rangle = 0$ and vari-

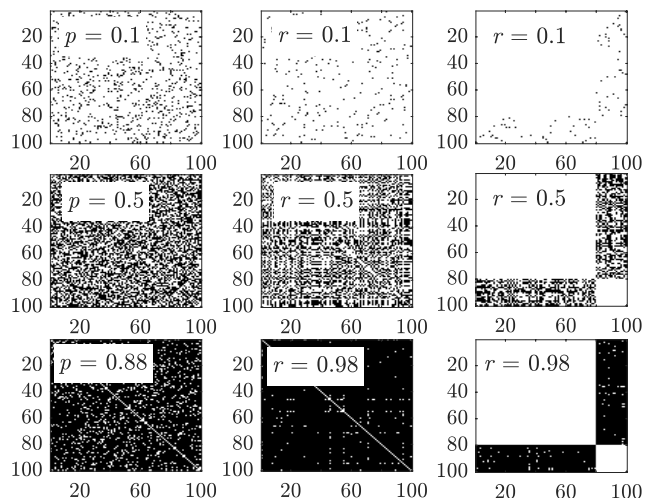


FIG. 1. Structure of Hamiltonian (1) for ERGs (first column), RGGs (second column), and BRGGs (third column). Three values of connection probability p and connection radius r are considered. For the BRGGs case, $s = 4N/5$.

ance $\langle |h_{nm}|^2 \rangle = (1 + \delta_{nm})/2$. In addition, each graph is assumed to be undirected i.e., $h_{nm} = h_{mn}$ such that $H = H^T$, with T the transpose operation. From the physical point of view, those weights, h_{nn} and h_{nm} , may represent respectively random self-loops and random strength interactions between vertices n and m .

As an example, in Fig. 1 the structure of Hamiltonian (1) is depicted for ERGs, RGGs, and BRGGs, in first, second, and third column, respectively. Different values of connection probability p and connection radius r are considered, as shown in the insets. The block structure of the Hamiltonian of BRGGs with $s = 4N/5$ is clearly different to those of ERGs and RGGs.

In the one open channel situation, the graphs are open to the outside by attaching to them a single-channel lead described by the following 1D tight-binding Hamiltonian

$$H_{\text{lead}} = \sum_{n=1}^{-\infty} (|n\rangle\langle n+1| + |n+1\rangle\langle n|). \quad (2)$$

In this case, due to the flux conservation condition, the scattering matrix, $S(E)$, reduces to a phase which can be written as [32, 54]

$$S(E) = e^{i\phi(E)} = 1 - 2i \sin(k) W^T \frac{1}{E - \mathcal{H}_{\text{eff}}} W, \quad (3)$$

where $k = \arccos(E/2)$ is the wave vector supported in the lead, E is the energy, and \mathcal{H}_{eff} is the non-Hermitian effective Hamiltonian given by

$$\mathcal{H}_{\text{eff}} = H - e^{ik} W W^T \quad (4)$$

with H the $N \times N$ tight-binding Hamiltonian matrix of Eq. (1) that describes the isolated graphs with N resonant states. In Eq. (3), W is an $N \times 1$ energy independent

matrix that couples the N resonant states to the single propagating mode in the lead. The elements of W are equal to zero or ε , where ε is the coupling strength between the graphs and the lead. Furthermore, assuming that the wave vector k undergoes slight changes near the energy band center, we set $E = 0$ and neglect the energy dependence of H_{eff} and S .

Since for ERGs and RGGs all the vertices are statistically equivalent, the single channel lead is attached to any vertex chosen at random. For BRGGs, however, as mentioned above, the vertices belong to two different disjoint sets, set A with s vertices and set B with $N - s$ vertices, that is, vertices are not equivalent and thus there are several possibilities to attach the single channel lead. If $s = N/2$, for instance, both sets have the same number of vertices and the set where the lead is attached is not relevant. In previous studies [26], it has been shown that several scattering and transport properties of weighted BRGGs(s) with $s = N/2$ and $N/5$ show good agreement with RMT predictions, then in this work we will consider the case $s = 4N/5$ with the single channel lead attached to the larger set; a setup where the RMT limit is not attained [26].

III. SCATTERING MEASURES

In this section, the scattering measures used to analyze the properties of ERGs, RGGs, and BRGGs are presented. These correspond to scattering phases, Wigner delay times, and resonance widths when the graphs support one open channel. The analysis is performed in the so-called perfect coupling regime between the graphs and the lead. Other transport properties when random graphs support more than one open channel were analyzed, for instance, in Refs. [25, 26].

A. Scattering phases and perfect coupling regime

Within the framework of RMT and in the one-channel situation, that is, when a single-channel lead is attached to the system (1), the scattering matrix reduces to a phase, $S(E) = e^{i\phi(E)}$ [see Eq. (3)], whose distribution is given by [55]

$$P(\phi) = \frac{1}{2\pi} \frac{1}{\gamma + \sqrt{\gamma^2 - 1} \cos \phi}, \quad (5)$$

in the diffusive (metallic-like) regime, where $\gamma = (1 + |\langle S \rangle|^2)/(1 - |\langle S \rangle|^2)$ and $\langle S \rangle$ is the average over an ensemble of S matrices. The averaged scattering matrix, $\langle S \rangle$, can be interpreted as the fraction of the incident waves which comes out promptly from the scattering region. Then, $\langle S \rangle$ provides a measure of the coupling strength between the system and external region [35, 56, 57]. In the perfect coupling regime, $\langle S \rangle$ vanishes and the phase is uniformly distributed over the unit circle. Here, the

analysis presented in next sections is performed in the perfect coupling regime between the graphs and the lead, that is, in the regime when $\langle S \rangle \approx 0$. This corresponds to the situation where none of the waves are reflected back promptly from the scattering region.

B. Wigner delay time and resonance widths

The delay experienced by a probe due to its interactions with a scattering region is well characterized by the so-called Wigner delay time τ [33, 34]. It is defined in terms of the scattering matrix S and its derivative with respect to the energy E . In the one channel case, near the center of the spectrum ($E = 0$), the Wigner delay time can be written as [42, 58]

$$\tau(E = 0) = \left. \frac{d\phi(E)}{dE} \right|_{E=0} = -2 \text{Im Tr}(E - H_{\text{eff}})^{-1} \Big|_{E=0}. \quad (6)$$

Furthermore, the poles of the scattering matrix show up as resonances which correspond to the complex eigenvalues $\mathcal{E}_n = E_n - i\Gamma/2$ of the effective non-Hermitian Hamiltonian H_{eff} [see Eq. (4)], where E_n and Γ_n are the position and width of the n th resonance, respectively. In addition, the lifetime of the n th resonance is related to the resonance width as $\tau_n = 1/\Gamma_n$.

For the graph models considered in this work, due to the random configuration of the vertices and also due to the random strength of interactions between vertices, both quantities, Wigner delay times and resonance widths, show sample-to-sample fluctuations. Therefore, in what follows, a statistical analysis over an ensemble of equivalent graphs shall be considered.

IV. RESULTS

For the statistical analysis of Wigner delay times and resonance widths Γ shown below, the calculations are performed near the center of the spectrum, i.e., close to $E \approx 0$ and under the perfect coupling regime between the graphs and the lead. **In addition, for the statistics of Γ , we use an eigenvalue window of about one-tenth of the total spectra around $E \approx 0$.** The graph sizes considered correspond to $N = 100, 200$, and 400 , with random realizations, or ensemble sizes, such that the statistics is fixed to 10^6 data. Also, the results displayed do not contain error bars since the statistics is performed with a large amount of data such that the error bars are smaller than the symbol size.

Prior to moving forward to the statistical analysis of Wigner delay times and of resonance widths of the random graphs under study, the perfect coupling condition between the graphs and the lead is first established. This condition is attained at the value of the coupling strength $\varepsilon = \varepsilon_0$ such that $\langle S(\varepsilon_0) \rangle \approx 0$. In this scenario, none of

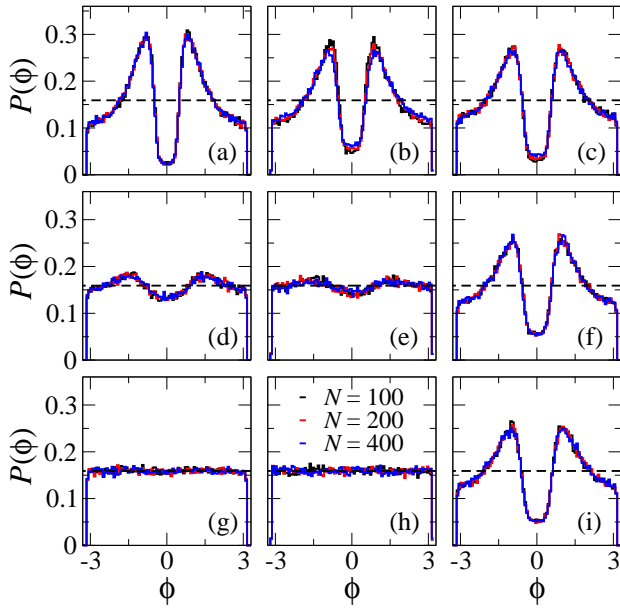


FIG. 2. Phase distribution in the perfect coupling regime for tight-binding ERGs (first column), RGGs (second column), and BRGGs($4N/5$) (third column). The graph sizes correspond to $N = 100, 200,$ and 400 , in black, red, and blue histograms. The scaling parameter is fixed to $\xi = 0.2$ ($0.2, 0.2$), 5.0 ($4.0, 1.8$), and 70.08 ($29.87, 6.59$) for ERGs (RGGs, BRGGs) shown in upper, middle, and lower panels. These values lead to nearly isolated, half connected, and mostly connected graphs, respectively. Horizontal black dashed lines correspond to the uniform distribution $P(\phi) = 1/2\pi$.

the waves are reflected back before entering the scattering region and, as a consequence, the internal structure of the scattering region can be probed.

In previous studies, a detailed numerical analysis of $\langle S \rangle$ as a function of ε and the average degree $\langle k \rangle$ shows that a coupling strength given by [25, 26]

$$\varepsilon_0 \approx \begin{cases} 0.462 \langle k \rangle^{0.29} + 0.374 & \text{for ERGs,} \\ 0.462 \langle k \rangle^{0.29} + 0.374 & \text{for RGGs,} \\ 0.760 \langle k \rangle^{0.02} + 0.060 & \text{for BRGGs}(4N/5), \end{cases} \quad (7)$$

sets the perfect coupling regime for ERGs, RGGs, and BRGGs, respectively, as a function of $\langle k \rangle$. That relation is independent of the graph sizes and of the number of attached leads, and it will be used in all our calculations to set the perfect coupling condition. Furthermore, a scaling analysis shows that the parameter

$$\xi = \langle k \rangle N^{-\alpha} \quad (8)$$

scales well a number of relevant scattering and transport properties [26], highlighting their universal character. For tight-binding ERGs, RGGs, and BRGGs($4N/5$), the exponents $\alpha = 0.075 \pm 0.0029, 0.26 \pm 0.0185,$ and 0.3429 ± 0.0371 , respectively, were obtained [26]. For BRGGs(s), other values of α can be obtained depending on the sizes of sets A and B.

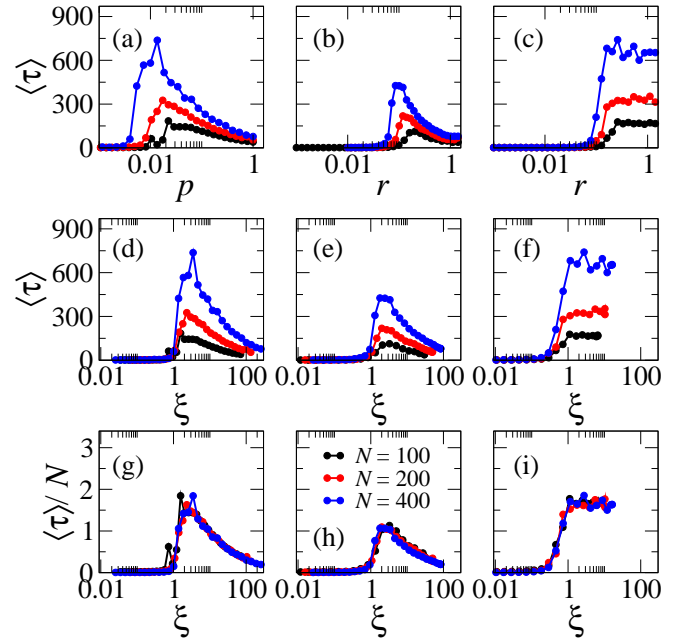


FIG. 3. Average Wigner delay time for tight-binding ERGs (first column), RGGs (second column), and BRGGs($4N/5$) (third column) as a function of the connection probability p and the connection radius r (upper panels), and as a function of scaling parameter ξ (middle and lower panels). The graph sizes N are indicated in panel (h). Each point is computed by averaging over 10^6 random realizations.

In the metallic-like or diffusive regime and under the perfect coupling condition, $\langle S \rangle \approx 0$, the phase of the S -matrix is uniformly distributed around $1/2\pi$, see Eq. (2). Therefore, a crossover towards uniformity is expected in the phase distribution of random graphs as a function of the average degree $\langle k \rangle$ or the scaling parameter ξ . This behavior is observed in Fig. 2 where the phase distribution for tight-binding ERGs, RGGs, and BRGGs, in left, middle, and right columns, respectively, is depicted considering three graph sizes, see panel (h). In each panel, the coupling strength ε_0 , such that $\langle S(\varepsilon_0) \rangle \approx 0$, is set for graphs with a scaling parameter ξ that leads to nearly isolated, half connected, and mostly connected graphs, in upper, middle, and lower panels, respectively. Those values correspond to $\xi = 0.2$ ($0.2, 0.2$), 5.0 ($4.0, 1.8$), and 70.08 ($29.87, 6.59$) for tight-binding ERGs (RGGs, BRGGs).

As observed in Fig. 2, the phase distribution scales well with ξ and the graphs size dependence drops off. That is, once ξ is fixed, $P(\phi)$ is also fixed. Also, in the metallic-like regime, i.e., for mostly connected graphs, the phase is uniformly distributed around $1/2\pi$ for ERGs and for RGGs, see Figs. 2 (g) and (h). For the case of BRGGs, the perfect coupling regime is not attained due to the lack of complexity in the graphs and the asymmetry of the scattering setup.

Once the perfect coupling condition is set, we now start our analysis by examining first the behavior of the

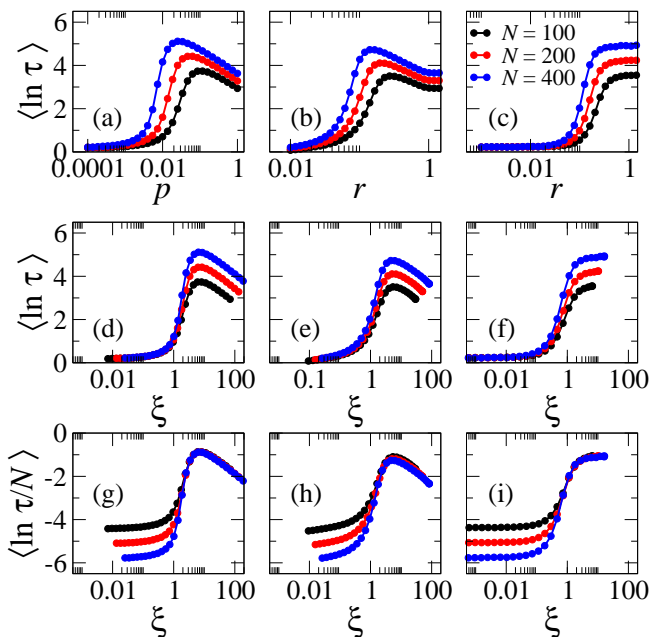


FIG. 4. Average of the logarithm of the Wigner delay time for tight-binding ERGs (first column), RGGs (second column), and BRGGs(4N/5) (third column) as a function of connection probability p and connection radius r (upper panels), and as a function of scaling parameter ξ (middle and lower panels). The results for three graphs sizes N are reported: $N = 100$, 200, and 400, in black, red, and blue full circles, respectively. In every panel, each data value is computed by averaging over 10^6 realizations of the corresponding random graph.

Wigner delay time as a function of the parameters of the graph models under study. Figure 3 shows the average Wigner delay time as a function of the connection probability p and the connection radius r in upper panels, and as a function of scaling parameter ξ in middle and lower panels for ERGs, RGGs, and BRGGs, in first, second, and third column, respectively. The average is performed over 10^6 realizations of random graphs. The graph sizes considered are indicated in panel (h). For nearly isolated graphs ($p \approx 0$ or $r \approx 0$), no time is spent by the electronic wave inside the media as shown in all panels of Fig. 3. As the graphs get more connected, the time spent inside the scattering media increases until it reaches a maximum for the connection probability $p \approx 0.01$, connection radius $r \approx 0.9$, and scaling parameter $\xi \approx 2.0$, respectively, as shown in each panel. Also, the larger the graph size N , the more time the wave spends inside the graphs, as observed in upper and middle panels. From their maximum time, the average Wigner delay time decreases as the graphs get mostly connected due to the appearance of multiple pathways. Furthermore, notice that even though the scaling parameter ξ scales well several scattering and transport properties of tight-binding ERGs, RGGs, and BRGGs [44], this parameter does not scale well the average Wigner delay time, as shown in middle and lower panels of Fig. 3. In order to find a scal-

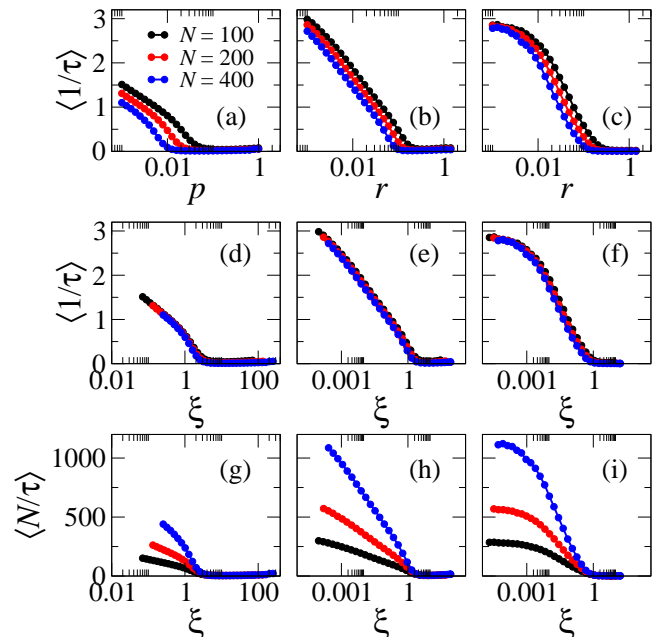


FIG. 5. Average of the inverse Wigner delay time for tight-binding ERGs (first column), RGGs (second column), and BRGGs(4N/5) (third column) as a function of connection probability p and connection radius r (upper panels), and as a function of the scaling parameter ξ (middle and lower panels). Three graphs sizes N are considered: $N = 100$, 200, and 400. In all panels, each data value is computed by averaging over 10^6 realizations of the corresponding random graph.

ing of $\langle \tau \rangle$, the average Wigner delay time is normalized by the graph size, as it is shown in the lower panels of Fig. 3 for the ERGs, RGGs, and BRGGs, in first, second, and third column, respectively. As observed, for the three graph sizes considered, the curves of $\langle \tau \rangle / N$ vs. ξ show a tendency to fall on top of each other where however, slight deviations are noticeable.

Also, further insight into the behavior of the Wigner delay time is provided by looking at its logarithm. For this purpose, the average of the logarithm of the Wigner delay time for ERGs, RGGs, and BRGGs, in first, second, and third column, respectively, as a function of p and r in upper panels, and as a function of scaling parameter ξ in middle and lower panels, is reported in Fig. 4. The graph sizes considered are indicated in the inset of panel (c). Since for very low values of p , r , or ξ the graphs mostly consist of isolated nodes, then no diffusion occurs and no time is spent by the electronic wave inside the graphs. As the connectivity increases, the wave spends more time within the scattering region until a maximum time is reached for ERGs and RGGs. However, for BRGGs the time spent by the wave inside the media keeps increasing as a function of connection radius r until its maximum is reached for complete bipartite graphs. As expected, the larger the graph size, the larger the time spent by the wave inside the media, as shown in panels (a-f). In order to scale this behavior, in

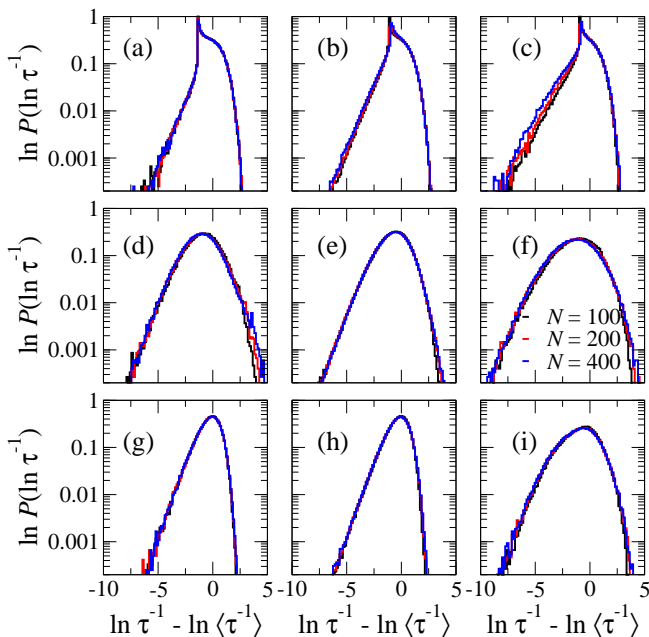


FIG. 6. Distribution of the logarithm of the inverse Wigner delay time for tight-binding ERGs (first column), RGGs (second column), and BRGGs($4N/5$) (third column). For the numerical results graphs sizes $N = 100, 200,$ and 400 , depicted in black, red, and blue, are considered. In upper, middle, and lower panels, the scaling parameter is fixed to $\xi = 0.2$ (0.2, 0.2), 5.0 (4.0, 1.8), and 70.08 (29.87, 6.59) for ERGs (RGGs, BRGGs), respectively. These values of ξ lead to graphs in the insulator, intermediate, and metallic regimes, respectively. As observed in lower panels, universal behavior is reached.

middle and lower panels of Fig. 4, $\langle \ln \tau \rangle$ and $\langle \ln(\tau/N) \rangle$ as a function of scaling parameter ξ , respectively, are depicted. As observed, ξ scales quite well the behavior of $\langle \ln \tau \rangle$ and that of $\langle \ln(\tau/N) \rangle$ for values of $\xi < 1$ and $\xi > 3$, respectively, of ERGs and RGGs. For BRGGs, ξ scales well the behavior of $\langle \ln(\tau/N) \rangle$ for values of $\xi > 1$. Even though, the parameter ξ scales reasonably well the behavior of τ , other relevant scattering and transport properties of tight-binding ERGs, RGGs, and BRGGs were shown to be properly scaled by ξ [44].

Moreover, in the one channel situation both the partial delay times and the proper delay times (defined as the energy derivative of phase shifts and in terms of the scattering matrix and its derivative with respect to the energy, respectively) are identical to the Wigner delay time. Since the joint distribution of the reciprocals of the proper delay times is known and given by the Laguerre ensemble [59], then it is instructive to study the behavior of the inverse of Wigner delay time too. Therefore, in Fig. 5, the average of the inverse of Wigner delay time for ERGs, RGGs, and BRGGs, in first, second, and third column, respectively, as a function of p and r in upper panels, and as a function of ξ in middle and lower panels, is reported. The graph sizes are indicated in panel (a).

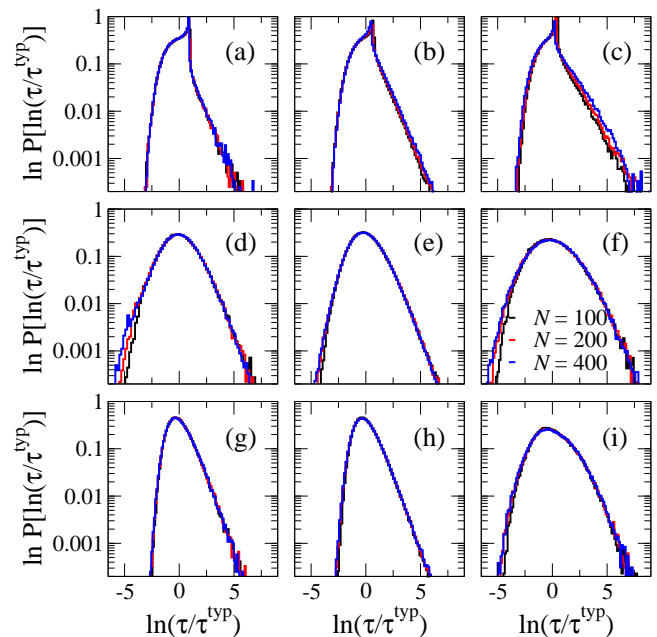


FIG. 7. Distribution of the logarithm of the Wigner delay time, normalized to its typical value, as a function of $\ln(\tau/\tau^{\text{typ}})$ for tight-binding ERGs (first column), RGGs (second column), and BRGGs($4N/5$) (third column). The numerical results are obtained considering graphs sizes $N = 100, 200,$ and 400 , depicted in black, red, and blue histograms. In upper, middle, and lower panels the scaling parameter is fixed to $\xi = 0.2$ (0.2, 0.2), 5.0 (4.0, 1.8), and 70.08 (29.87, 6.59) for tight-binding ERGs (RGGs, BRGGs), respectively. These values of ξ lead to graphs in the insulator, intermediate, and metallic regimes, respectively. As observed in lower panels, universal behavior is attained for fully connected graphs.

In every panel, each point is computed by averaging over 10^6 realizations of the corresponding random graphs.

Upper panels of Fig. 5 show that as p or r increases, the average of the inverse of Wigner delay time decreases, i.e., the time spent by the electronic wave inside the scattering media increases until it reaches its maximum (minimum of $\langle 1/\tau \rangle$). This indicates the localization of the electronic wave where conduction is suppressed. Also, the larger the graph size N , the faster the decay of the average inverse delay time. The graph size dependence is almost absent when plotting $\langle 1/\tau \rangle$ as a function of ξ for ERGs and BRGGs for values of $\xi < 1$ with slight deviations noticeable for $\xi > 1$, see panels (d) and (f). However, the scaling parameter ξ does not scale well the average of inverse Wigner delay time for RGGs, see panel (e). Now, notice that a better scaling is obtained for values of $\xi > 1$ when plotting $\langle N/\tau \rangle$ vs ξ for the three graph models under consideration, as shown in panels (g), (h), and (i) for ERGs, RGGs, and BRGGs, respectively. A similar panorama is also observed for different bipartitions of BRGGs(s), for instance when $s = N/2$ and $N/5$ (not shown here).

In what follows, we focus on the distribution of the

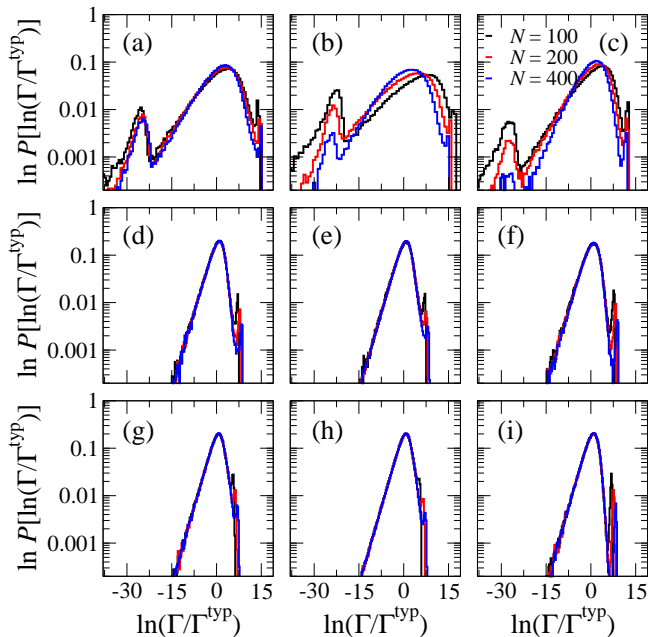


FIG. 8. $\ln P[\ln(\Gamma/\Gamma^{\text{typ}})]$ as a function of $\ln(\Gamma/\Gamma^{\text{typ}})$ for tight-binding ERGs (first column), RGGs (second column), and BRGGs($4N/5$) (third column). The numerical results correspond to graphs sizes $N = 100, 200,$ and 400 , depicted in black, red, and blue histograms. In upper, middle, and lower panels, the scaling parameter is fixed to $\xi = 1.5 (1.5, 0.8), 5.0 (4.0, 2.0),$ and $70.08 (29.87, 6.59)$ for ERGs (RGGs, BRGGs), respectively, which lead to graphs in the insulator, in between the insulator-to-metallic, and in the metallic regimes. A tendency to universal behavior as the graphs get more connected is observed.

inverse Wigner delay time and of the Wigner delay time normalized to its typical value. As it is reported below, both distributions show universal behavior for graphs in a wide range of transport regimes when scaled by the parameter ξ . Figure 6 shows the distribution of the logarithm of the inverse Wigner delay time for tight-binding ERGs (first column), RGGs (second column), and BRGGs($4N/5$) (third column), considering three graph sizes as indicated in panel (f). In upper, middle, and lower panels, the scaling parameter ξ is fixed to values that lead to graphs into the insulator, in between the insulator-to-metallic, and in the metallic regimes, respectively. Those values correspond to $\xi = 0.2 (0.2, 0.2), 5.0 (4.0, 1.8),$ and $70.08 (29.87, 6.59)$ for tight-binding ERGs (RGGs, BRGGs), respectively. As observed, there exists a slight dependence on the graph size in the distribution of $\ln P(\ln \tau^{-1})$ for very low connected graphs, or for graphs in the insulator regime; particularly for BRGGs; see panel (c). This dependency is diminished as the graphs get more connected until a universal behavior is reached. At this stage, the scaling parameter ξ scales well the behavior of $\ln P(\ln \tau^{-1})$, see lower panels. This trend to universal behavior is attained from half-connected to mostly connected graphs,

as shown in middle and lower panels of Fig. 6.

In an equivalent way, the tendency to universal behavior can also be observed in the distribution of the logarithm of the Wigner delay time, normalized to its typical value $\tau^{\text{typ}} \equiv \exp(\ln \tau)$. This behavior is reported in Fig. 7 which shows $\ln P(\ln \tau/\tau^{\text{typ}})$ as a function of $\ln(\tau/\tau^{\text{typ}})$ for the three graph models: ERGs (first column), RGGs (second column), and BRGGs (third column). Again, three graph sizes are considered as indicated in panel (f). As in Fig. 6, the scaling parameter is fixed to $\xi = 0.2 (0.2, 0.2), 5.0 (4.0, 1.8),$ and $70.08 (29.87, 6.59)$ for tight-binding ERGs (RGGs, BRGGs), respectively, which leads to graphs in the insulator (upper panels), in between the insulator-to-metallic (middle panels), and in the metallic regimes (lower panels). As observed in lower panels, all the curves fall on top of each other. This highlights the universal character of $\ln P(\ln \tau/\tau^{\text{typ}})$, or equivalently of $\ln P(\ln \tau^{-1})$.

Finally, a quantity highly related to the Wigner delay time is the resonance width whose reciprocal describes the lifetime of a particle in a resonant state escaping into the open channel. Figure 8 reports the distribution of the logarithm of the resonance widths $\ln P[\ln(\Gamma/\Gamma^{\text{typ}})]$, normalized to its typical value $\Gamma^{\text{typ}} \equiv \exp(\ln \Gamma)$. Right, middle, and left columns show the results considering tight-binding ERGs, RGGs, and BRGGs, respectively, with the graph sizes indicated in panel (c). In upper, middle, and lower panels, the scaling parameter is fixed to $\xi = 1.5 (1.5, 0.8), 5.0 (4.0, 2.0),$ and $70.08 (29.87, 6.59)$ for ERGs (RGGs, BRGGs), respectively, that sets graphs in the insulator, in between the insulator-to-metallic, and in the metallic regimes. Opposite to the cases previously considered, for the analysis of resonance widths, the parameter ξ is fixed to $\xi = 1.5$ to set graphs in the insulator-like regime. Also, even though some deviations appear for graphs in the insulator regime, or for low connected graphs (see upper panels), a tendency to universal behavior of $\ln P[\ln(\Gamma/\Gamma^{\text{typ}})]$ is clearly observed as the graphs get more connected (see middle and lower panels).

V. CONCLUSIONS

From the scattering matrix approach to electronic transport and from the equivalence established between the adjacency matrix and the tight-binding Hamiltonian matrix describing, respectively, a random graph and an electronic media, a numerical analysis of the Wigner delay times and the resonance widths of tight-binding Erdős-Rényi random graphs, random geometric graphs, and bipartite random geometric graphs, has been presented. The Wigner delay times and the resonance widths are related to the delay experienced by a probe due to interactions with a scattering media and provide important information about the internal dynamics inside that media. Our results show that the distribution of both quantities, Wigner delay times and resonance widths, for random graphs with a single channel lead

attached perfectly to them, are invariant under a scaling parameter ξ which depends on the average degree and the graph size; see Eq. (8). That is, universal behavior in the distribution of Wigner delay times and resonance widths is observed when scaled by ξ . Even though the graph models considered in this work do not possess critical properties in the sense of an Anderson transition (i.e. here we observe a smooth crossover from localization to diffusion by increasing ξ), it is worth mentioning that such crossover can be well captured by the Wigner delay time, a transport property which is very convenient from an experimental point of view since direct access to the eigenfunctions of the scattering media is not required. Also our results may be experimentally verified in photonic systems in the microwave regime which emulate tight-binding models. Specifically, the 2D photonic

arrays reported in Refs. [48, 49, 52] can be seen as a photonic tight-binding realization of random geometric graphs.

ACKNOWLEDGMENTS

L.A.R.-L. gratefully acknowledges the financial support from CONAHCyT (Mexico), through the Grant No. 775585, and from the French government, through the UCA ^{JEDI} Investments in the Future project managed by the National Research Agency (ANR) with the reference number ANR-15-IDEX-0001. A.M.M.-A. acknowledges financial support from CONAHCyT under the program “Estancias Posdoctorales por México 2022”. J.A.M.-B. thanks support from VIEP-BUAP (Grant No. 100405811-VIEP2024), Mexico.

-
- [1] S. H. Strogatz, *Nature* **410**, 268 (2001)
- [2] S. N. Dorogovtsev and J. F. F. Mendes, *Adv. Phys.* **51**, 1079 (2001)
- [3] R. Albert and A. L. Barabási, *Rev. Mod. Phys.* **74**, 47 (2002)
- [4] M. E. J. Newman, *SIAM Rev.* **45**, 167 (2003)
- [5] S. Boccaletti, V. Latora, Y. Moreno, M. Chavez, D.-U. Hwang, *Phys. Rep.* **424**, 175 (2006)
- [6] R. Durrett, *Random Graph Dynamics* (Cambridge University Press, UK, 2007)
- [7] V. Latora, V. Nicosia, and G. Russo, *Complex Networks Principles, Methods and Applications* (Cambridge University Press, UK, 2017)
- [8] E. Estrada, *The Structure of Complex Networks: Theory and Applications* (Oxford University Press, New York, 2011).
- [9] M. Penrose, *Random Geometric Graphs* (Oxford University Press, New York, 2003)
- [10] P. Erdős and A. Rényi, *Publicationes Mathematicae* **6**, 290 (1959)
- [11] G. Cimini, T. Squartini, F. Saracco, D. Garlaschelli, A. Gabrielli, and G. Caldarelli, *Nat. Rev. Phys.* **1**, 58 (2019)
- [12] A. Ozkanlar and A. E. Clark, *J. Compt. Chem.* **35**, 495 (2014)
- [13] S. N. Dorogovtsev and A. V. Goltsev, *Rev. Mod. Phys.* **80**, 1275 (2008)
- [14] E. Estrada, N. Hatano, and M. Benzi, *Phys. Rep.* **514**, 89 (2012)
- [15] A. L. Barabási and R. Albert, *Science* **286**, 509 (1999)
- [16] D. S. Callaway, M. E. J. Newman, S. H. Strogatz, and D. J. Watts, *Phys. Rev. Lett.* **25**, 5468 (2000)
- [17] K.-I. Goh, B. Kahng, and D. Kim, *Phys. Rev. E* **64**, 051903 (2001)
- [18] G. J. Rodgers, K. Austin, B. Kahng, and D. Kim, *J. Phys. A: Math. Gen.* **38**, 9431 (2005)
- [19] B. Georgeot, O. Giraud, and D. L. Shepelyansky, *Phys. Rev. E* **81**, 056109 (2010)
- [20] S. Jalan, G. Zhu, and B. Li, *Phys. Rev. E* **84**, 046107 (2011)
- [21] I. Farkas, I. Derényi, H. Jeong, Z. Nédá, Z. N. Oltvai, E. Ravasz, A. Schubert, A. L. Barabási, and T. Vicsek, *Physica A* **314**, 25 (2002)
- [22] S. N. Dorogovtsev, A. V. Goltsev, J. F. F. Mendes, and A. N. Samukhin, *Phys. Rev. E* **68**, 046109 (2003)
- [23] E. López, S. V. Buldyrev, S. Havlin, and H. E. Stanley, *Phys. Rev. Lett.* **94**, 248701 (2005).
- [24] Y. Xue, J. Wang, L. Li, D. He, and B. Hu, *Phys. Rev. E* **81**, 037101 (2010)
- [25] A. J. Martínez-Mendoza, A. Alcazar-López, and J. A. Méndez-Bermúdez, *Phys. Rev. E* **88**, 012126 (2013)
- [26] A. M. Martínez-Argüello, K. B. Hidalgo-Castro, and J. A. Méndez-Bermúdez, *ArXiv:2310.03936v1*
- [27] R. Aguilar-Sánchez, J. A. Méndez-Bermúdez, F. A. Rodrigues, and J. M. Sigarreta, *Phys. Rev. E* **102**, 042306 (2020)
- [28] M. Sade, T. Kalisky, S. Havlin, and R. Berkovits, *Phys. Rev. E* **72**, 066123 (2005)
- [29] J. N. Bandyopadhyay and S. Jalan, *Phys. Rev. E* **76**, 026109 (2007)
- [30] S. Jalan and J. N. Bandyopadhyay, *Phys. Rev. E* **76**, 046107 (2007)
- [31] S. Jalan, N. Solymosi, G. Vattay, and B. Li, *Phys. Rev. E* **81**, 046118 (2010)
- [32] C. W. J. Beenakker, *Rev. Mod. Phys.* **69**, 731 (1997)
- [33] E. P. Wigner, *Phys. Rev.* **98**, 145 (1955)
- [34] F.T. Smith, *Phys. Rev.* **118**, 349 (1960)
- [35] Y. V. Fyodorov and H.-J. Sommers, *J. Math. Phys.* **38**, 1918 (1997)
- [36] Y. V. Fyodorov, D. V. Savin, and H.-J. Sommers, *Phys. Rev. E* **55**, R4857(R) (1997)
- [37] A. M. Martínez-Argüello, A. A. Fernández-Marín, and M. Martínez-Mares, *Eur. Phys. J. Spec. Top.* **226**, 519 (2017)
- [38] Y. V. Fyodorov and D. V. Savin, *Phys. Rev. Lett.* **108**, 184101 (2012)
- [39] M. Novaes, *Europhys. Lett.* **139**, 21001 (2022)
- [40] L. Chen, S. M. Anlage, and Y. V. Fyodorov, *Phys. Rev. E* **103**, L050203 (2021)
- [41] L. Chen, S. M. Anlage, and Y. V. Fyodorov, *Phys. Rev. Lett.* **127**, 204101 (2021)
- [42] T. Kottos and M. Weiss, *Phys. Rev. Lett.* **89**, 056401 (2002)

- [43] J. A. Méndez-Bermúdez and T. Kottos, Phys. Rev. B **72**, 064108 (2005)
- [44] A. M. Martínez-Argüello, M. Carrera-Núñez, and J. A. Méndez-Bermúdez, Phys. Rev. E **107**, 024139 (2023).
- [45] C. Zhong, S. M. Arisona, X. Huang, M. Batty, and G. Schmitt, Int. J. Geogr. Inf. Sci. **28**, 2178 (2014)
- [46] C. Stegehuis, L. Weedage, Physica A **586**, 126460 (2022)
- [47] M. Barthélemy, Phys. Rep. **499**, 1 (2011)
- [48] U. Kuhl, S. Barkhofen, T. Tudorovskiy, H.-J. Stöckmann, T. Hossain, L. de Forges de Parny, and F. Mortessagne, Phys. Rev. B **82**, 094308 (2010)
- [49] S. Bittner, B. Dietz, M. Miski-Oglu, P. Oria Iriarte, A. Richter, and F. Schäfer, Phys. Rev. B **82**, 014301 (2010)
- [50] M. Bellec, U. Kuhl, G. Montambaux, and F. Mortessagne, Phys. Rev. B **88**, 115437 (2013)
- [51] S. Barkhofen, M. Bellec, U. Kuhl, and F. Mortessagne, Phys. Rev. B **87**, 035101 (2013)
- [52] G. J. Aubry, L. S. Froufe-Pérez, U. Kuhl, O. Legrand, F. Scheffold, and F. Mortessagne, Phys. Rev. Lett. **125**, 127402 (2020)
- [53] J. Dall and M. Christensen, Phys. Rev. E **66**, 016121 (2002)
- [54] J. J. M. Verbaarschot, H. A. Weidenmüller, and M. R. Zirnbauer, Phys. Rep. **129**, 367 (1985)
- [55] A. Ossipov and Y. V. Fyodorov, Phys. Rev. B **71**, 125133 (2005)
- [56] H. Feshbach, *Topics in the theory of nuclear reactions*, in Reaction Dynamics, edited by E. W. Montroll, G. H. Vineyard, M. Levy, and P. T. Matthews (Gordon and Breach, New York, 1973)
- [57] P. W. Brouwer and C. W. J. Beenakker, Phys. Rev. B **55**, 4695 (1997)
- [58] F. Steinbach, A. Ossipov, T. Kottos, and T. Geisel, Phys. Rev. Lett. **85**, 4426 (2000)
- [59] P. W. Brouwer, K. M. Frahm, C. W. J. Beenakker, Phys. Rev. Lett. **78**, 4737 (1997)